Copy
RM L56J15a

RESEARCH MEMORANDUM

EXPERIMENTAL STATIC AERODYNAMIC FORCES AND MOMENTS AT HIGH SUBSONIC SPEEDS ON A CANARD MISSILE DURING SIMULATED LAUNCHING FROM THE MIDSEMISPAN LOCATION OF A 45° SWEPTBACK WING-FUSELAGE-PYLON COMBINATION AT ZERO SIDESLIP

By William J. Alford, Jr., and Thomas J. King, Jr.

Langley Aeronautical Laboratory
Langley Field, Va.

CLASSIFIED DOCUMENT

NATIONAL ADVISORY COMMITTEE
FOR AERONAUTICS

WASHINGTON

January 14, 1957

NATIONAL ADVISORY COMMITTEE FOR AERONAUTICS

RESEARCH MEMORANDUM

EXPERIMENTAL STATIC AERODYNAMIC FORCES AND MOMENTS AT HIGH SUBSONIC SPEEDS ON A CANARD MISSILE DURING SIMULATED LAUNCHING FROM THE MIDSEMISPAN LOCATION OF A 45° SWEPTBACK WING-FUSELAGE-PYLON COMBINATION AT ZERO SIDESLIP

By William J. Alford, Jr., and Thomas J. King, Jr.

SUMMARY

An investigation was made at high subsonic speeds in the Langley high-speed 7- by 10-foot tunnel to determine the static aerodynamic forces and moments on a canard missile model during simulated launching from the midsemispan location of a 45° sweptback wing-fuselage-pylon combination. The results indicated significant variations in all the aerodynamic components with changes in chordwise location of the missile. Increasing the angle of attack caused increases in the induced effects on the missile model due to the wing-fuselage-pylon combination. Increasing the Mach number had little effect on the variation of the missile aerodynamic components with angle of attack except that non-linearities were incurred at smaller angles of attack for the higher Mach numbers. The effects of finite-wing thickness on the missile forces and moments at zero angle of attack increased with increasing Mach number.

A comparison of the results of this investigation with those in NACA RM L56J05 for a missile with tail located rearward of the center of gravity indicated that the canard missile forces and moments were affected by chordwise position, angle of attack, and Mach number in much the same manner although the variations differed in detail.

INTRODUCTION

The National Advisory Committee for Aeronautics is conducting investigations to determine the nature and origin of the mutual interference effects experienced by various combinations of wing-fuselage models and externally carried missiles. Previous investigations (refs. 1 to 5) have shown the existence of the generally objectionable interference effects, and references 1 and 2 have shown that they are primarily due, at low speed, to the nonuniform flow field generated in the vicinity of the airplane. The severity of these induced effects on the force and moment characteristics of a conventional missile (tail rearward of center of gravity) at high subsonic speeds has been reported in reference 6.

The purpose of the present paper is to present the results of an experimental investigation made at high subsonic speeds to determine the static aerodynamic forces and moments on a canard missile model during simulated launching from the midsemispan location of a 45° swept-back wing-fuselage-pylon combination. In order to expedite publication of these data only a brief analysis is presented.

SYMBOLS

C_N missile normal-force coefficient, $\frac{\text{Normal force}}{qS_m}$

C_m missile pitching-moment coefficient, $\frac{\text{Pitching moment}}{qS_m\bar{c}_m}$

C_Y missile side-force coefficient, $\frac{\text{Side force}}{qS_m}$

C_n missile yawing-moment coefficient, $\frac{\text{Yawing moment}}{qS_m b_m}$

C_l missile rolling-moment coefficient, $\frac{\text{Rolling moment}}{qS_m b_m}$

$C_{L,A}$ wing-fuselage lift coefficient, $\frac{\text{Lift}}{qS_A}$

q free-stream dynamic pressure, lb/sq ft

l_s unsupported missile sting length, ft (fig. 1)

S_m	exposed missile wing area of two panels, 0.0179 sq ft
S_A	airplane wing area, 2.25 sq ft
b_m	span of missile wings, 0.255 ft
b	span of wing-fuselage combination, ft
c	local wing chord of airplane model, ft
$\bar{c}_m$	mean aerodynamic chord of exposed missile wing area, 0.113 ft
$\bar{c}_A$	mean aerodynamic chord of airplane wing, 0.822 ft
C_P	pylon chord, ft
r	radius of missile body (fig. 2)
x	chordwise distance from leading edge of the local wing chord to missile center of gravity (positive rearward), ft
x_m	axial distance from missile nose (fig. 2)
y	spanwise distance from fuselage center line to missile center line (positive to right), ft
z	vertical distance from wing-chord plane to missile center line (positive up), ft
α	angle of attack, deg
β	angle of lateral skew of the missile relative to fuselage center line, deg
M	Mach number
V	free-stream velocity, ft/sec

MODELS AND APPARATUS

The wing of the wing-fuselage combination (fig. 1) used as the test vehicle had a quarter-chord sweepback of 45°, an aspect ratio of 4.0, a taper ratio of 0.30, and NACA 65A006 airfoil sections

[redacted]

parallel to the fuselage center line. The fuselage (ordinates given in table I) consisted of an ogival nose section, a cylindrical center section, and a truncated tail cone.

The canard missile model employed a cruciform arrangement of its wings and canard fins and is shown in figure 1 as part of the test setup. Details of the missile model are shown in figure 2. The pylon used in this investigation had an elliptic nose section, a flat center section, and a straight tapered trailing edge. The ordinates of the pylon are given in table II.

The missile model was internally instrumented with a five-component strain-gage balance and was supported from the rear of the wing-fuselage combination by a sting that was adjustable in the longitudinal plane. The missile center line was located 16 percent of the local wing chord below the one-half semispan station of the wing-fuselage combination and was translated through a range of chordwise locations.

TESTS

The tests were made in the Langley high-speed 7- by 10-foot tunnel at Mach numbers of 0.60, 0.80, 0.90, and 0.94 with the corresponding Reynolds number varying from 3.3 to 3.8 $\times 10^6$ per foot of a typical dimension. The variation of average Reynolds number with test Mach number is presented in figure 3. The angle-of-attack range generally extended at $M = 0.60$ from -2° to 18°, although at the higher Mach numbers the angle range was restricted by the load limit of the strain-gage balance and therefore varied with the loadings measured for each location of the missile. The tests were made at zero sideslip with the missile model located under the left wing of the wing-fuselage-pylon combination. The direction of positive angles and forces and moments of the missile model are as shown in figure 4.

CORRECTIONS AND ACCURACY

Blocking corrections applied to Mach number and dynamic pressure were determined by the method of reference 7. Jet-boundary corrections applied to the angle of attack were calculated by the method of reference 8.

Because of the flexibility characteristics of the missile sting and balance combination, changes are incurred in the missile angular and locational positions, in both the longitudinal and lateral planes, as a result of the aerodynamic loads and moments. Corrections have been

[redacted]

applied to the missile angle of attack to account for the deflection of both the major sting used to support the wing-fuselage-missile combination (see ref. 6) and the missile support sting and balance combination (fig. 1). The variation of the corrected angle of attack of the wing-fuselage combination with reference angle of attack due to the major sting deflection under load and due to jet-boundary considerations is presented in figure 5.

The variations in missile angle of attack due to the missile sting and balance combination are presented in figure 6 and a list of the missile sting lengths for the various chordwise locations investigated is presented in table III. In order to keep the unsupported sting length to a minimum, the missile sting was clamped to the pylon for positions where the missile model was ahead of the pylon leading edge. Because of the difference in the flexibility characteristics of the main support sting and the missile sting, there existed an incidence angle between the missile model and the wing-fuselage-pylon combination. A study of the deflection characteristics of the two support systems indicated that maximum angle of incidence was of the order of 1.6°. The magnitude of the angle of incidence may be determined for any chordwise location and angle of attack from the data presented in figure 6 and table III along with the aerodynamic force and moment data of the missile model. No corrections have been applied to the missile lateral angle, or the vertical and lateral locations because of the deflections of the missile sting and balance. A calibration of these deflections has been made and the results are presented in figure 6.

A study of the strain-gage-balance calibrations of the missile model and general repeatability of the test data indicates that the accuracy levels of the various force and moments are approximately as follows:

C_N	± 0.05
C_m	± 0.05
C_Y	± 0.05
C_n	± 0.05
C_l	± 0.01

RESULTS AND DISCUSSION

In analyzing the force and moment characteristics of the missile model it should be kept in mind that the missile was located beneath the left wing of the wing-fuselage-pylon combination and that the positive directions of angles, forces, and moments are as shown in figure 4.

[redacted]

The aerodynamic characteristics of the isolated missile model as determined from tests in the free stream are presented in figure 7. Although breakdown tests of the isolated missile were not obtained in the present investigation, this information may be obtained from reference 9. The aerodynamic characteristics of the missile model when in the presence of the wing-fuselage-pylon combination, at zero sideslip, are presented in figure 8 as a function of angle of attack for several Mach numbers and longitudinal locations. The lift characteristics of the isolated wing-fuselage combination are presented for orientation in figure 9.

The effects of varying the chordwise location of the missile relative to the leading edge of the local wing chord (fig. 8) were to cause significant variations in all the aerodynamic force and moment components. For the most forward missile center-of-gravity location ($x/c = -1.02$, fig. 8(i)) the missile is seen to be the least affected by the presence of the wing-fuselage-pylon combination although the force and moment levels have not reached their free-stream levels (fig. 7). This fact is consistent with the low-speed investigation reported in reference 3 wherein the missile was translated approximately 1.5 chord lengths before the free-stream conditions were reached.

Increasing the angle of attack (fig. 8) causes increases in the induced effects on the missile model due to the wing-fuselage-pylon combination. This can be explained from references 1, 2, and 9 as being due to the increase in wing circulation strength which results in increases in the magnitude of the downwash and sidewash angularity in conjunction with changes in the nonuniform dynamic pressure field.

Increasing the Mach number (fig. 8) had, in general, little effect on the variations of the missile aerodynamic characteristics with angle of attack, except that nonlinearities were incurred at smaller angles of attack for the higher Mach numbers. The flow disturbance effects due to finite-wing thickness increase with increasing Mach number as evidenced by the displacement of the missile force and moment curves at zero angle of attack. This result is in accord with theoretical predictions of the effects of Mach number on the flow-field characteristics at zero lift (ref. 10).

A comparison of the results of this investigation with those in reference 6 for a missile with tail located rearward of the center of gravity indicated that the canard missile forces and moments were affected by chordwise position, angle of attack, and Mach number in much the same manner although the variation differed in detail.

[redacted]

CONCLUDING REMARKS

The results of an experimental investigation made at high subsonic speeds to determine the static aerodynamic forces and moments on a canard missile during simulated launching from the midsemispan location of a 45° sweptback wing-fuselage-pylon combination indicate significant variations in all the aerodynamic components with changes in chordwise location of the missile. Increasing the angle of attack caused increases in the induced effects on the missile model due to the wing-fuselage-pylon combination. Increasing the Mach number had little effect on the variation of the missile aerodynamic components with angle of attack, except that nonlinearities were incurred at smaller angles of attack for the higher Mach numbers. The effects of finite-wing thickness on the missile forces and moments at zero angle of attack increased with increasing Mach number.

A comparison of the results of this investigation with those in NACA RM L56J05 for a missile with tail located rearward of the center of gravity indicated that the canard missile forces and moments were affected by chordwise position, angle of attack, and Mach number in much the same manner although the variations differed in detail.

Langley Aeronautical Laboratory,
National Advisory Committee for Aeronautics,
Langley Field, Va., September 27, 1956.

REFERENCES

1. Alford, William J., Jr., Silvers, H. Norman, and King, Thomas J., Jr.: Preliminary Low-Speed Wind-Tunnel Investigation of Some Aspects of the Aerodynamic Problems Associated With Missiles Carried Externally in Positions Near Airplane Wings. NACA RM L54J20, 1954.

2. Alford, William J., Jr.: Effects of Wing-Fuselage Flow Fields on Missile Loads at Subsonic Speeds. NACA RM L55E10a, 1955.

3. Alford, William J., Jr., Silvers, H. Norman, and King, Thomas J., Jr.: Experimental Aerodynamic Forces and Moments of Low Speed of a Missile Model During Simulated Launching From the Midsemispan Location of a 45° Sweptback Wing-Fuselage Combination. NACA RM L54K11a, 1955.

4. Alford, William J., Jr.: Experimental Static Aerodynamic Forces and Moments at Low Speed on a Canard Missile During Simulated Launching From the Midsemispan and Wing-Tip Locations of a 45° Sweptback Wing-Fuselage Combination. NACA RM L55A12, 1955.

5. Alford, William J., Jr., Silvers, H. Norman, and King, Thomas J., Jr.: Experimental Static Aerodynamic Forces and Moments at Low Speed on a Missile Model During Simulated Launching From the 25-Percent-Semispan and Wing-Tip Locations of a 45° Sweptback Wing-Fuselage Combination. NACA RM L55D20, 1955.

6. Alford, William J., Jr., and King, Thomas J., Jr.: Experimental Static Aerodynamic Forces and Moments at High Subsonic Speeds on a Missile Model During Simulated Launching From the Midsemispan Location of a 45° Sweptback Wing-Fuselage-Pylon Combination. NACA RM L56J05, 1956.

7. Herriot, John G.: Blockage Corrections for Three-Dimensional-Flow Closed-Throat Wind Tunnels, With Consideration of the Effect of Compressibility. NACA Rep. 955, 1950. (Supersedes NACA RM A7B28.)

8. Gillis, Clarence L., Polhamus, Edward C., and Gray, Joseph L., Jr.: Charts for Determining Jet-Boundary Corrections for Complete Models in 7- by 10-Foot Closed Rectangular Wind Tunnels. NACA WR L-123, 1945. (Formerly NACA ARR L5G31.)

9. Rubinstein, Marvin: Report of Force and Moment Tests of an 11% Scale Complete Model of the XASM-N-7 Bullpup Missile at Mach Numbers From .60 to 2.25. USCEC Rep. 32-1-4 (Aerod. Test Div., NAMTC, Pt. Mugu), Univ. of Southern California Eng. Center, Apr. 15, 1955.

[redacted]

10. Alford, William J., Jr.: Theoretical and Experimental Investigation of the Subsonic-Flow Fields Beneath Swept and Unswept Wings With Tables of Vortex-Induced Velocities. NACA TN 3738, 1956.

TABLE I.- FUSELAGE ORDINATES

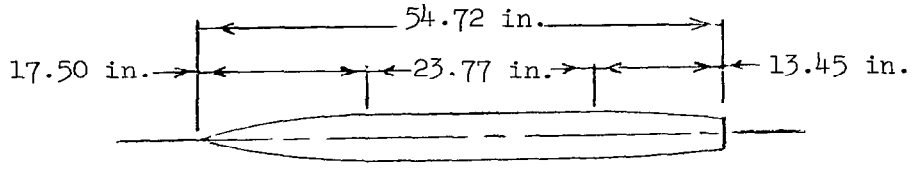

Ordinates, in.	
Station	Radius
0	0
2.00	.53
4.00	1.00
6.00	1.44
8.00	1.80
10.00	2.07
12.00	2.30
14.00	2.42
16.00	2.47
17.50	2.50
41.27	2.50
43.27	2.42
45.27	2.35
47.27	2.25
48.30	2.14
54.72	1.65

[redacted]

TABLE II.- PYLON ORDINATES

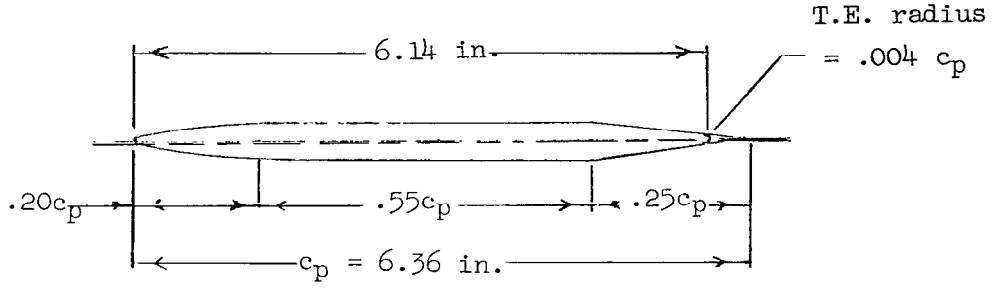

Ordinates, percent chord	
x	±y
0	0
2.5	1.45
5.0	2.00
15.0	2.90
20.0	3.00
75.0	3.00
Straight taper	
100.0	0

[redacted]

TABLE III.- MISSILE STING LENGTHS

Missile center-of-gravity location, x/c	Effective sting length, $l_s/\bar{c}_A$ (*)
Isolated missile	2.00
0.51	1.23
.38	1.39
.15	1.56
0	.79
-.15	.92
-.34	1.09
-.57	1.30
-.79	1.50
-1.02	1.71

*For missile center-of-gravity locations $x/c = 0$ through $x/c = -1.02$, the missile sting was clamped to pylon of wing-fuselage-pylon combination.

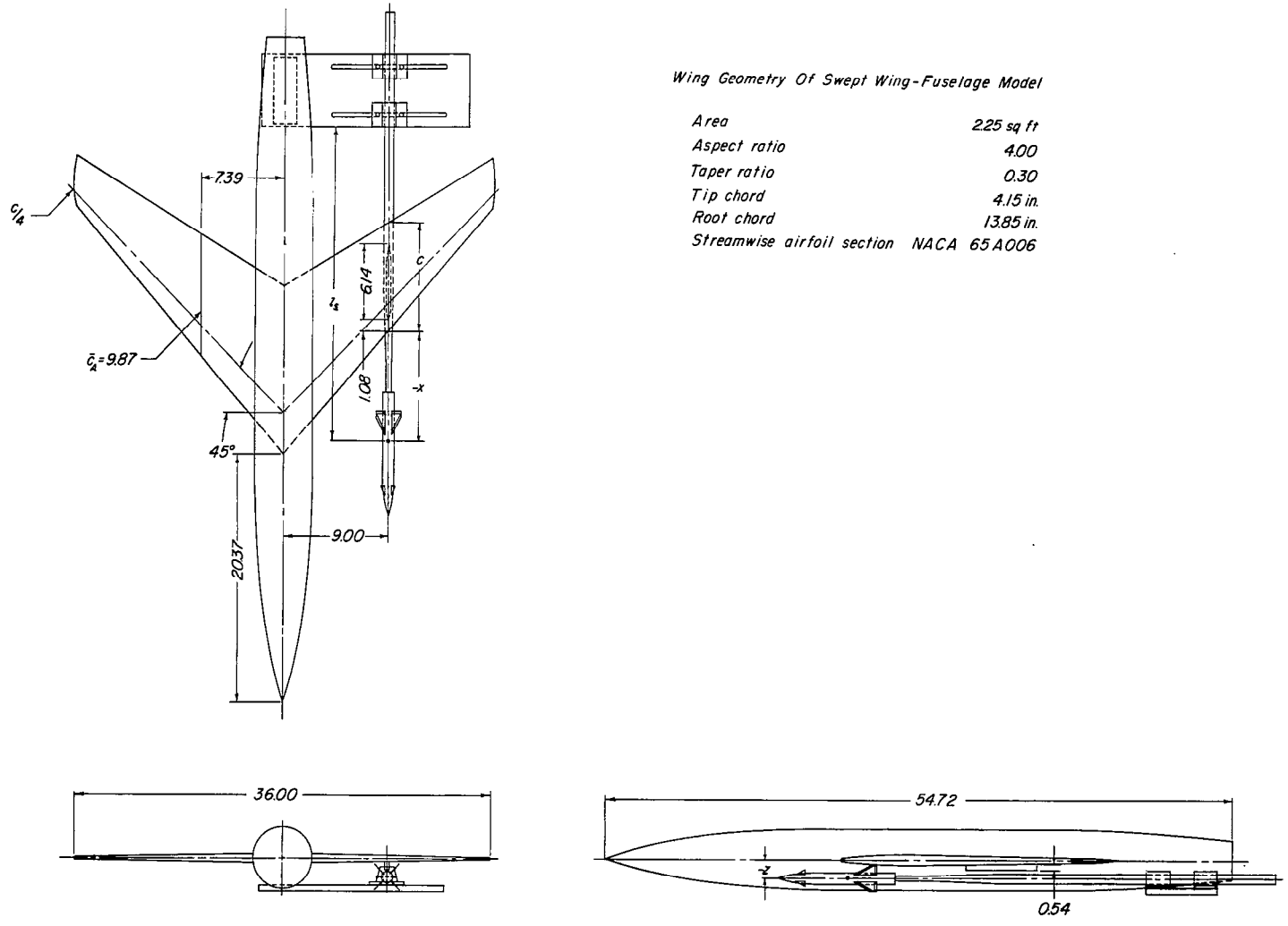

Wing Geometry Of Swept Wing-Fuselage Model

Area	2.25 sq ft
Aspect ratio	4.00
Taper ratio	0.30
Tip chord	4.15 in.
Root chord	13.85 in.
Streamwise airfoil section	NACA 65A006

Figure 1.- Three-view drawing of wing-fuselage model with missile model installed. All dimensions in inches.

Nose ordinates, inches	
x_m	r
0	0
.312	.105
.624	.186
.935	.258
1.25	.318
1.56	.371
1.87	.412
2.18	.444
2.50	.469
2.81	.483
3.12	.486

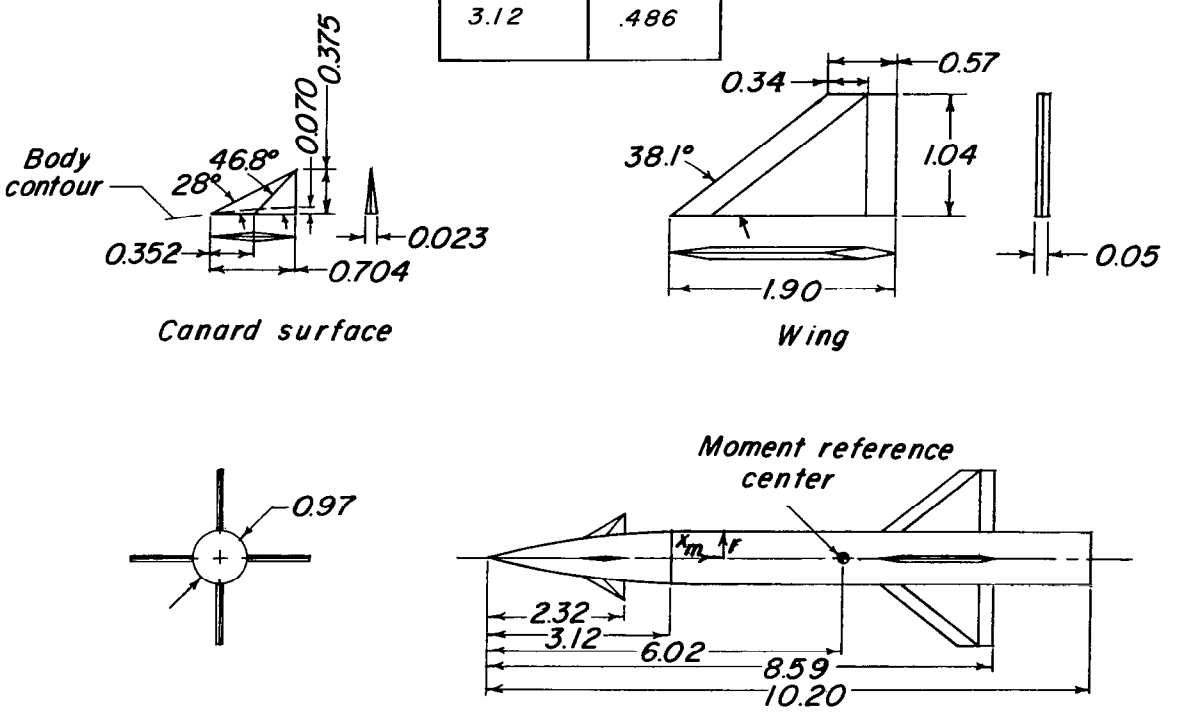

Figure 2.- Drawing of missile model. All linear dimensions in inches.

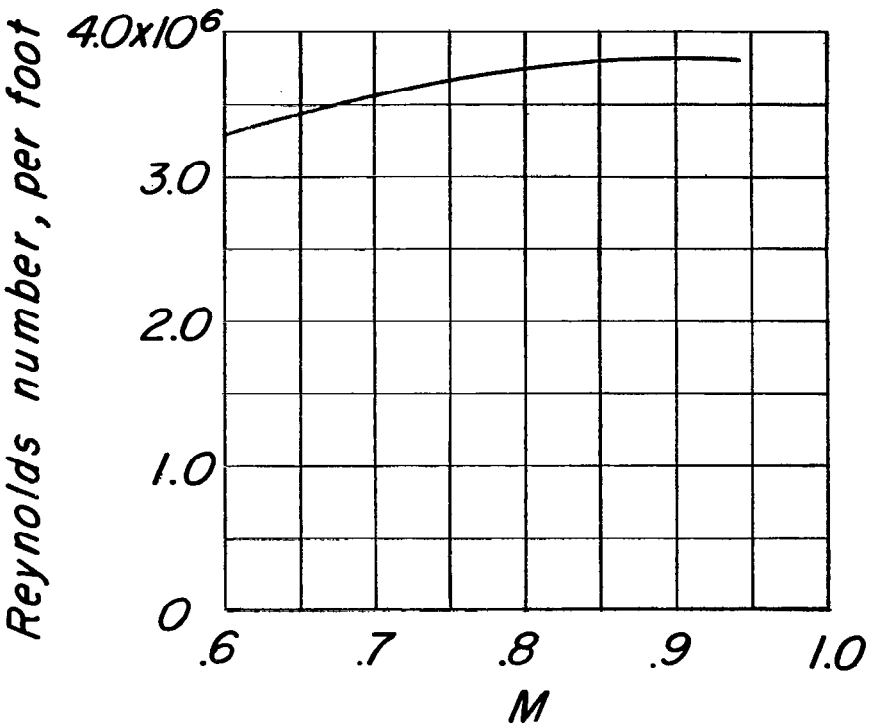

Figure 3.- Variation of average Reynolds number with test Mach number.

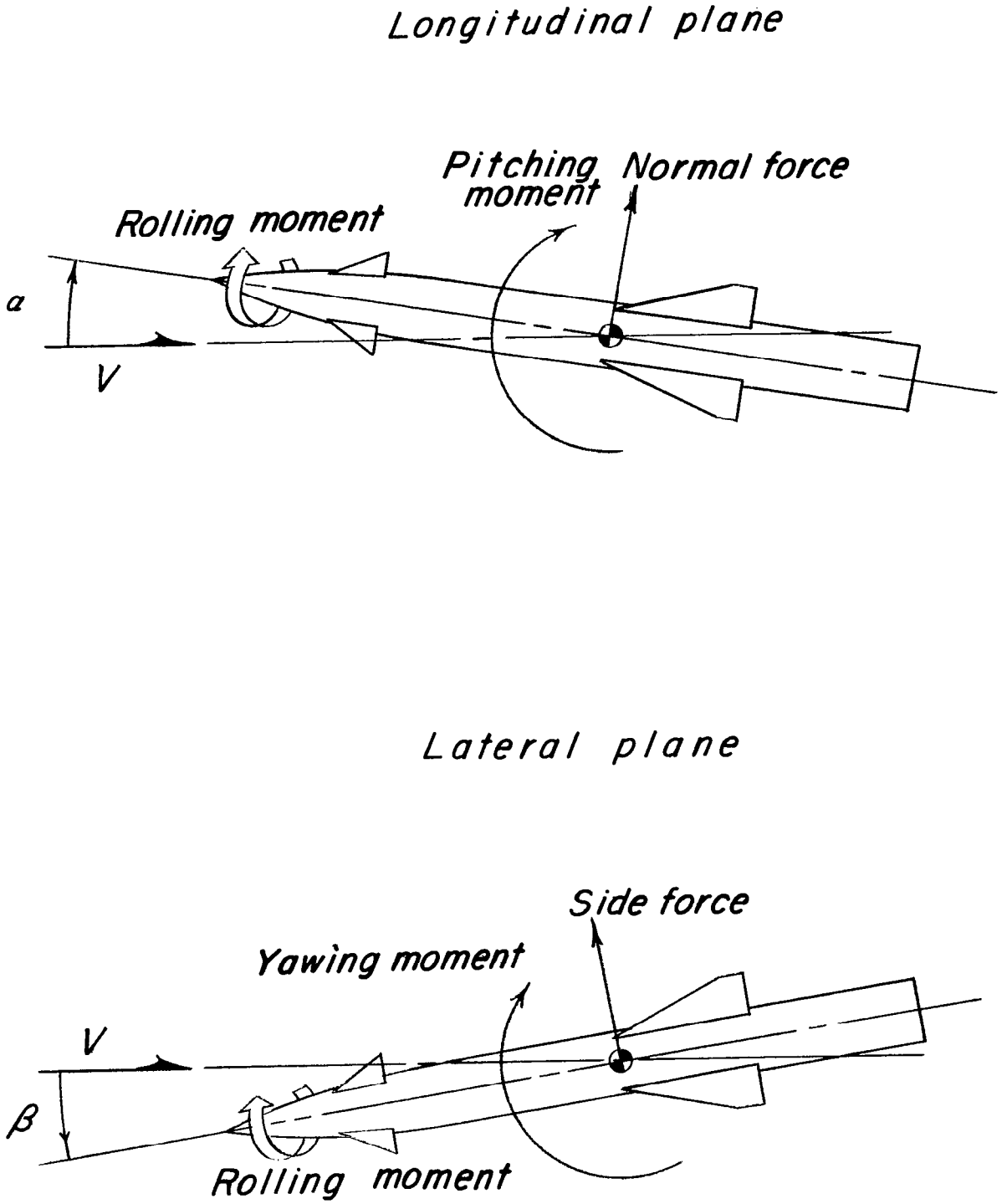

Figure 4.- Positive directions of forces and moments as measured on missile.

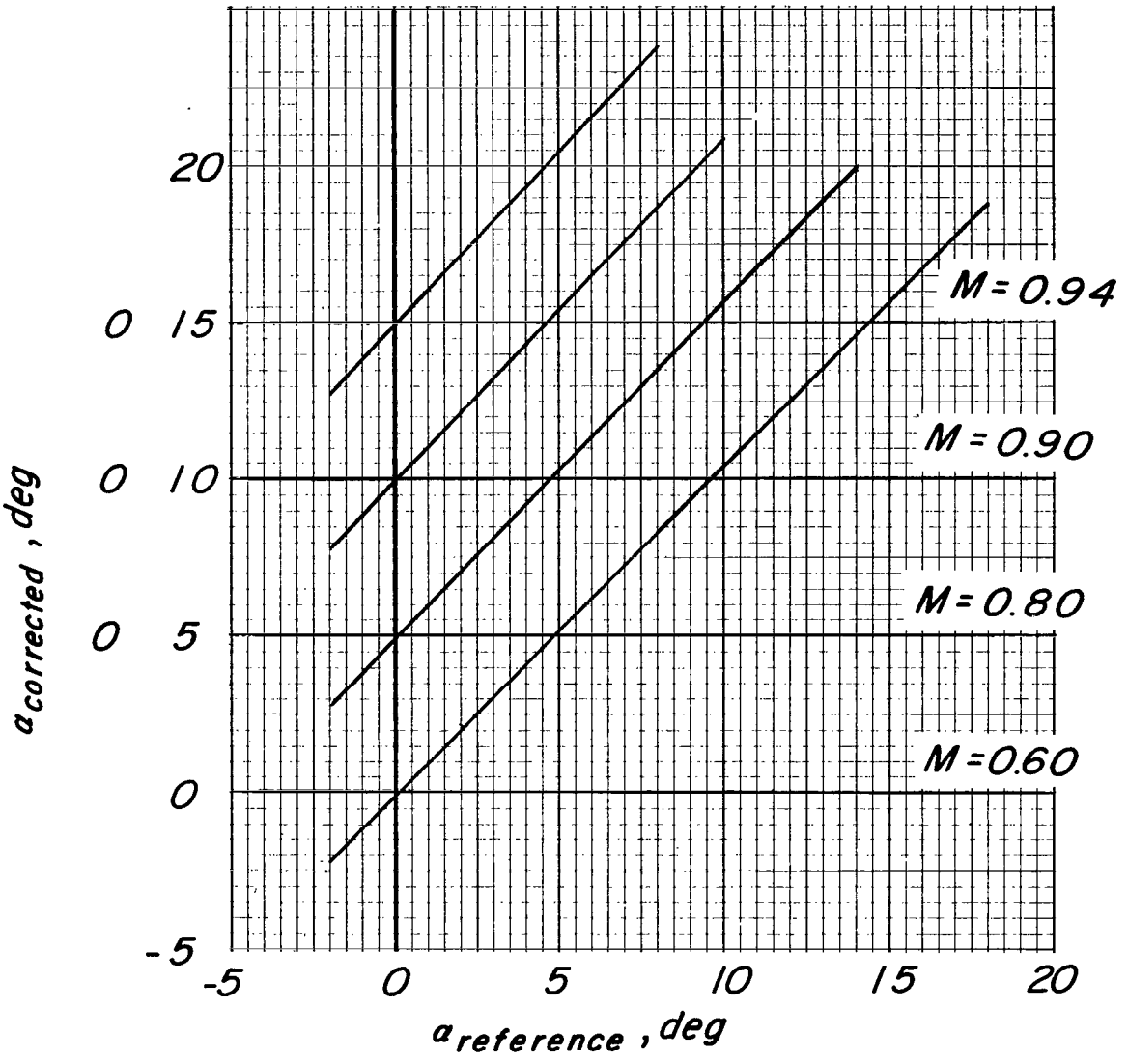

Figure 5.- Variation of corrected angle of attack of wing-fuselage model with reference angle of attack.

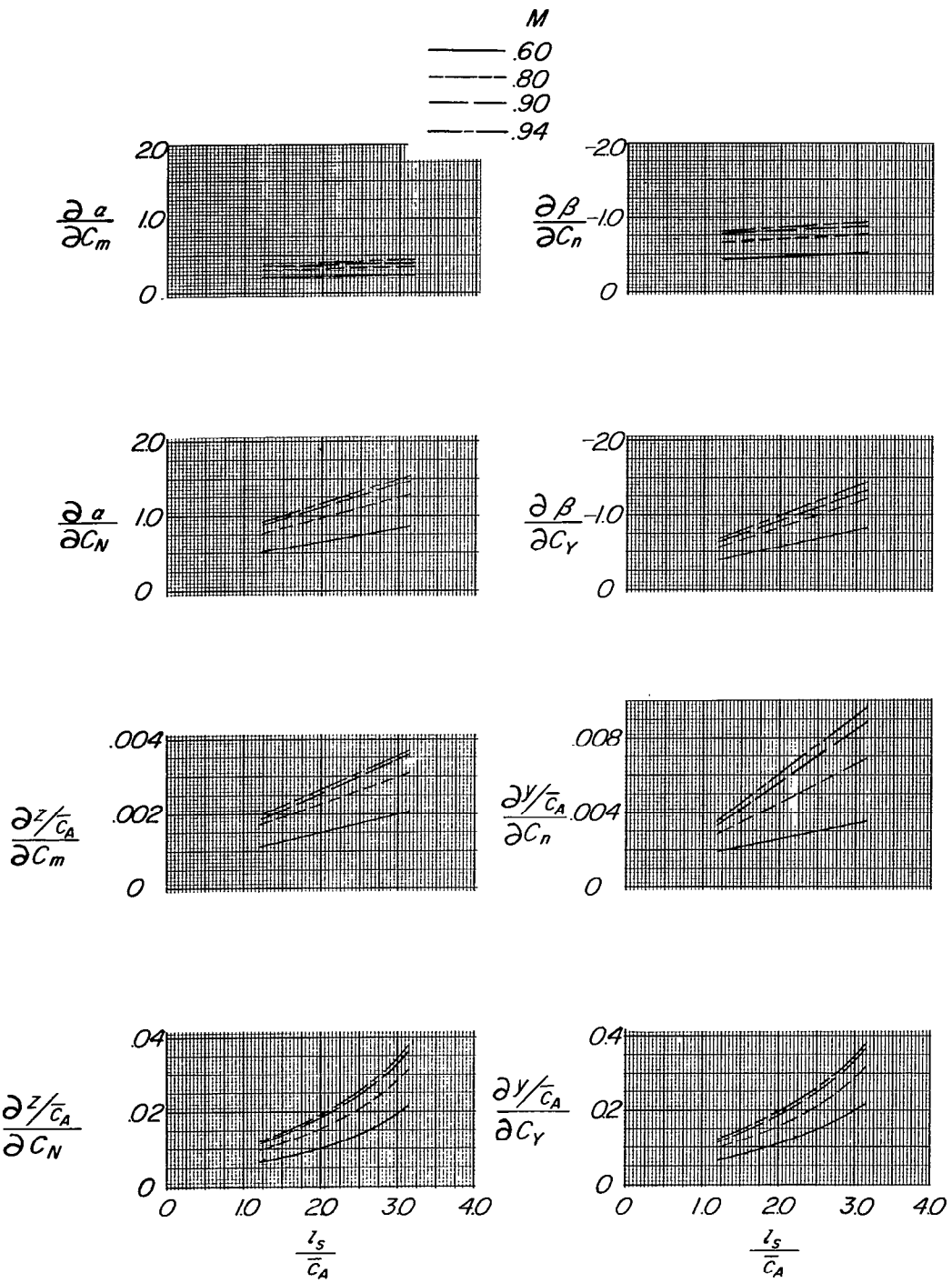

Figure 6.- Deflection characteristics of missile sting and balance combination (angular deflections in degrees).

[redacted]

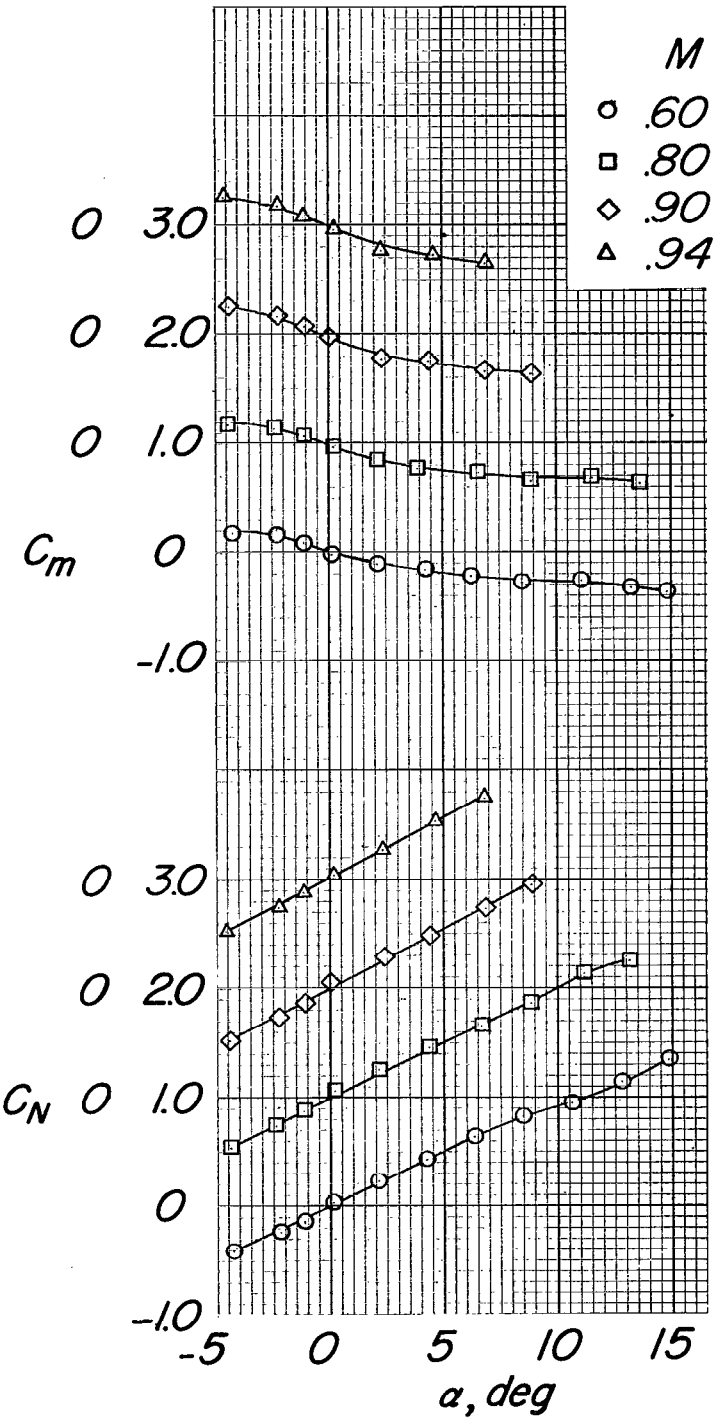

Figure 7.- Aerodynamic forces and moments of the isolated missile model.

[redacted]

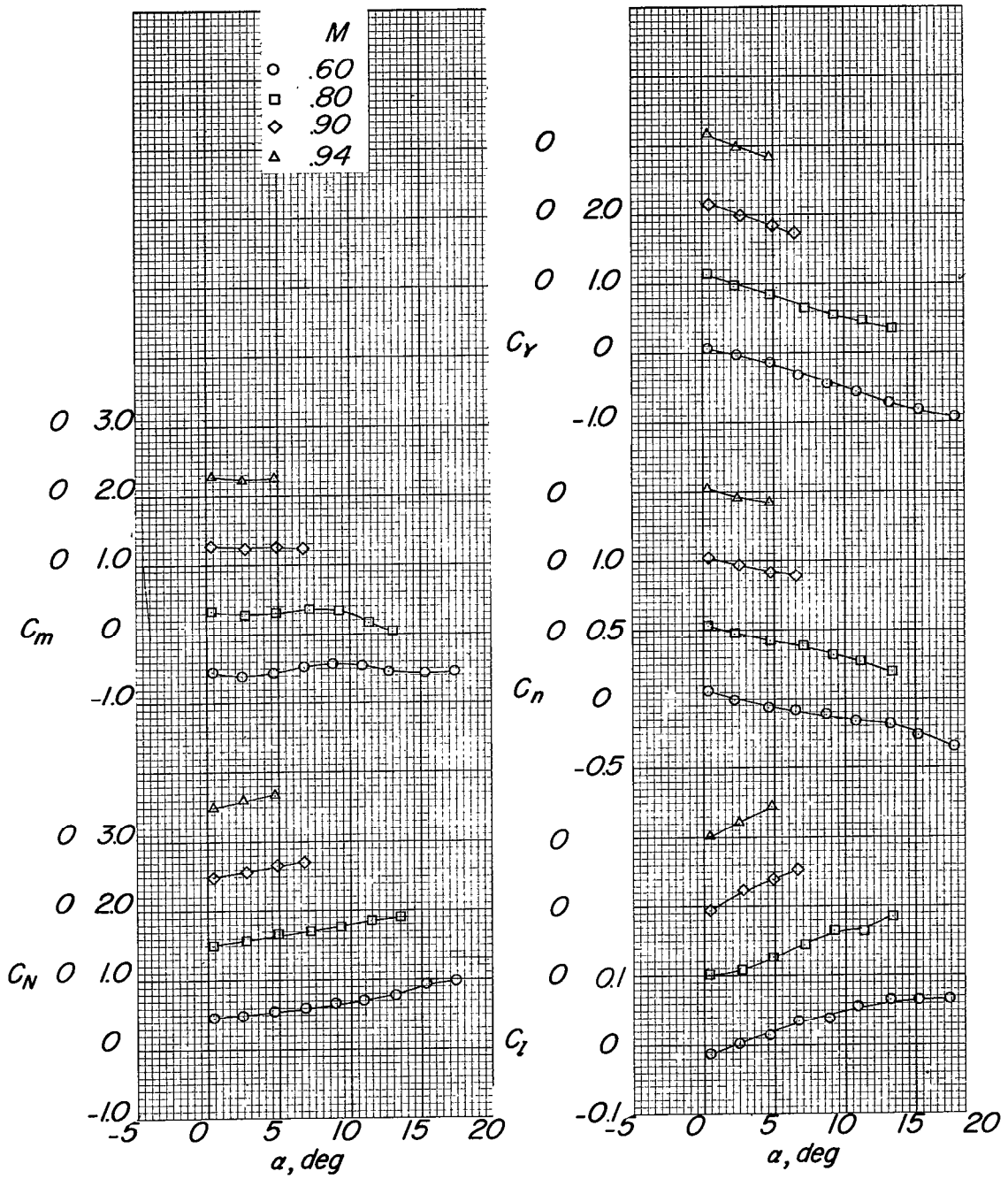

(a) x/c = 0.51.

Figure 8.- Missile aerodynamic forces and moments in presence of wing-fuselage-pylon combination for various Mach numbers; z/c = -0.16.

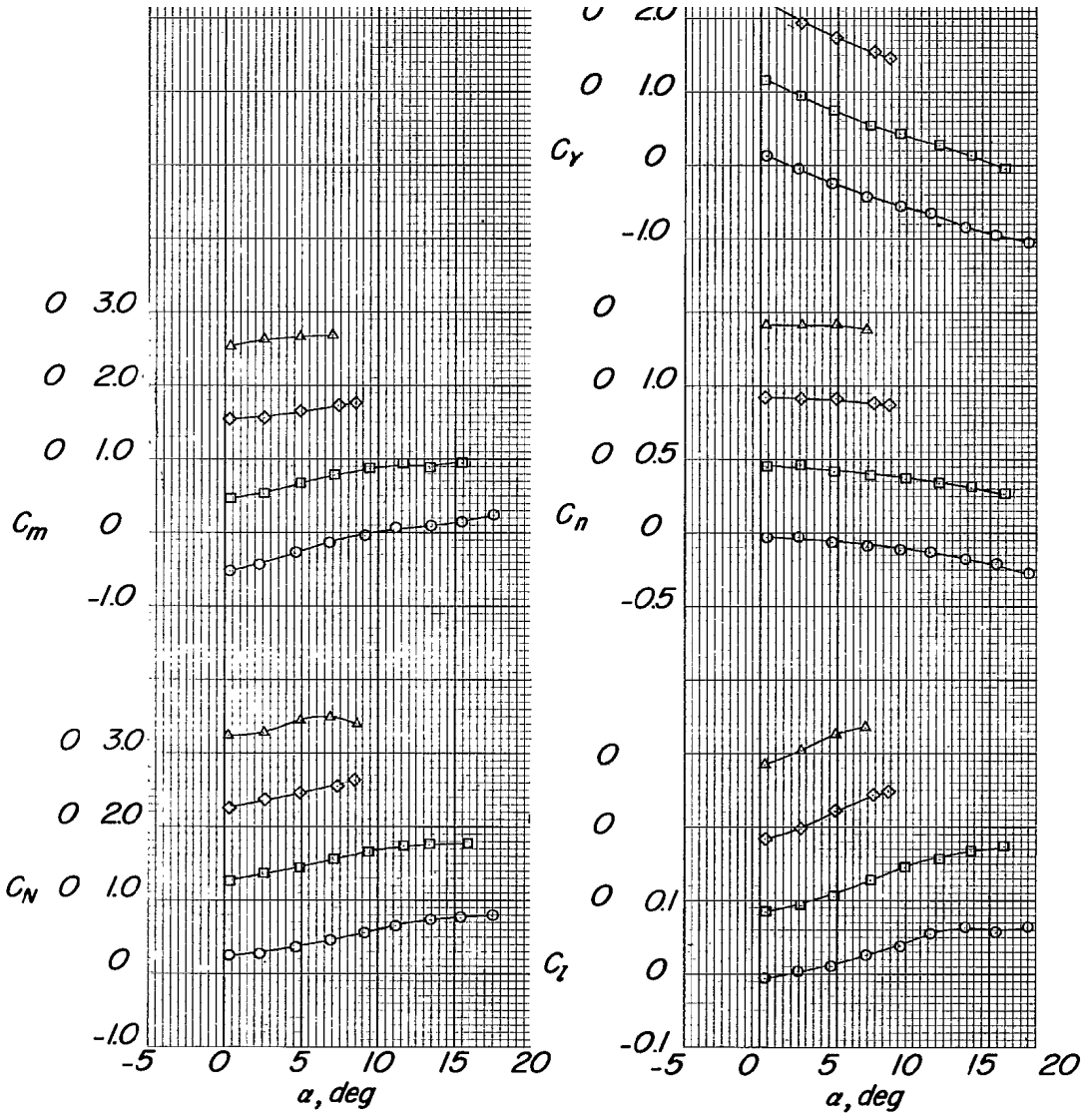

(b) x/c = 0.38.

Figure 8.- Continued.

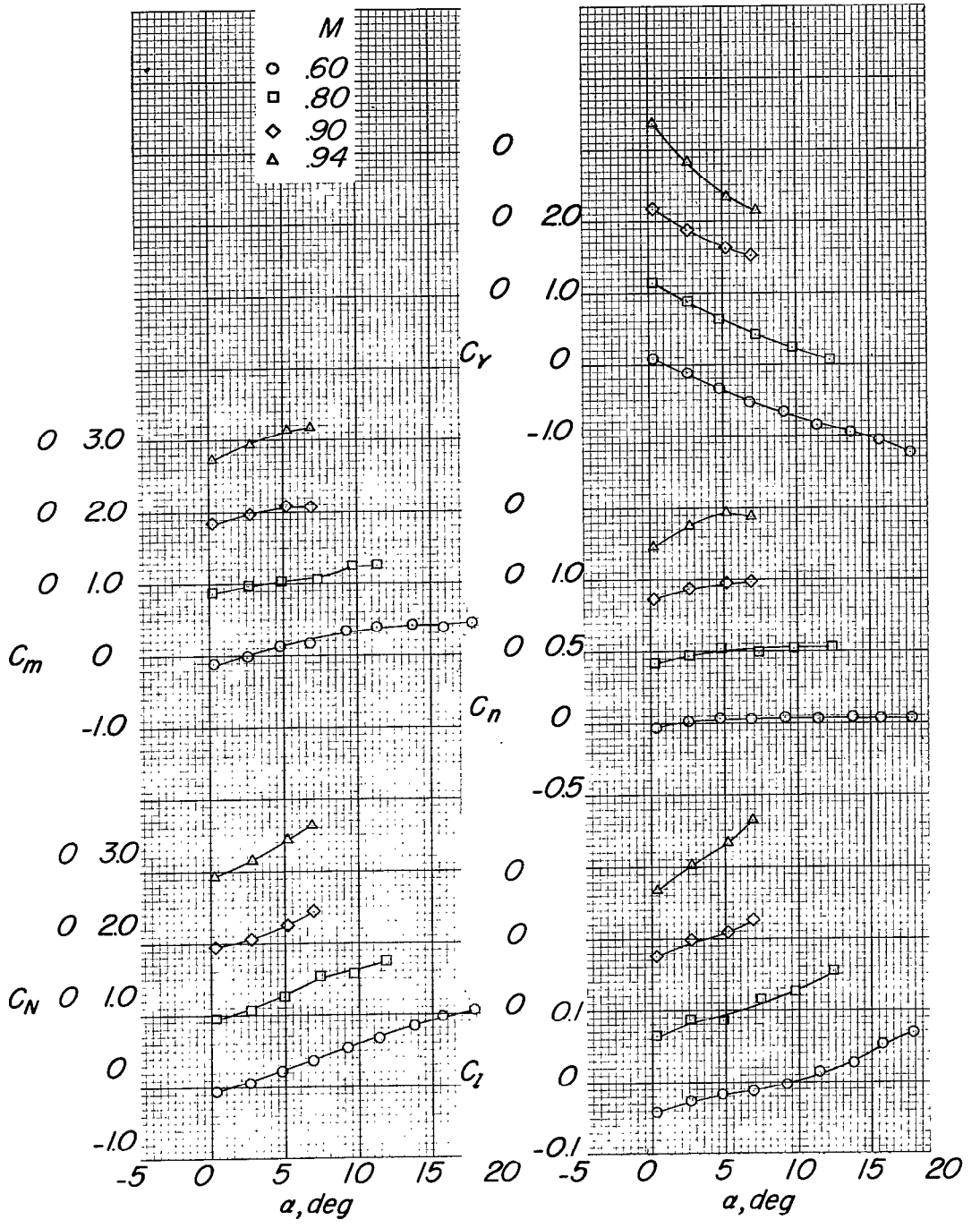

(c) x/c = 0.15.

Figure 8.- Continued.

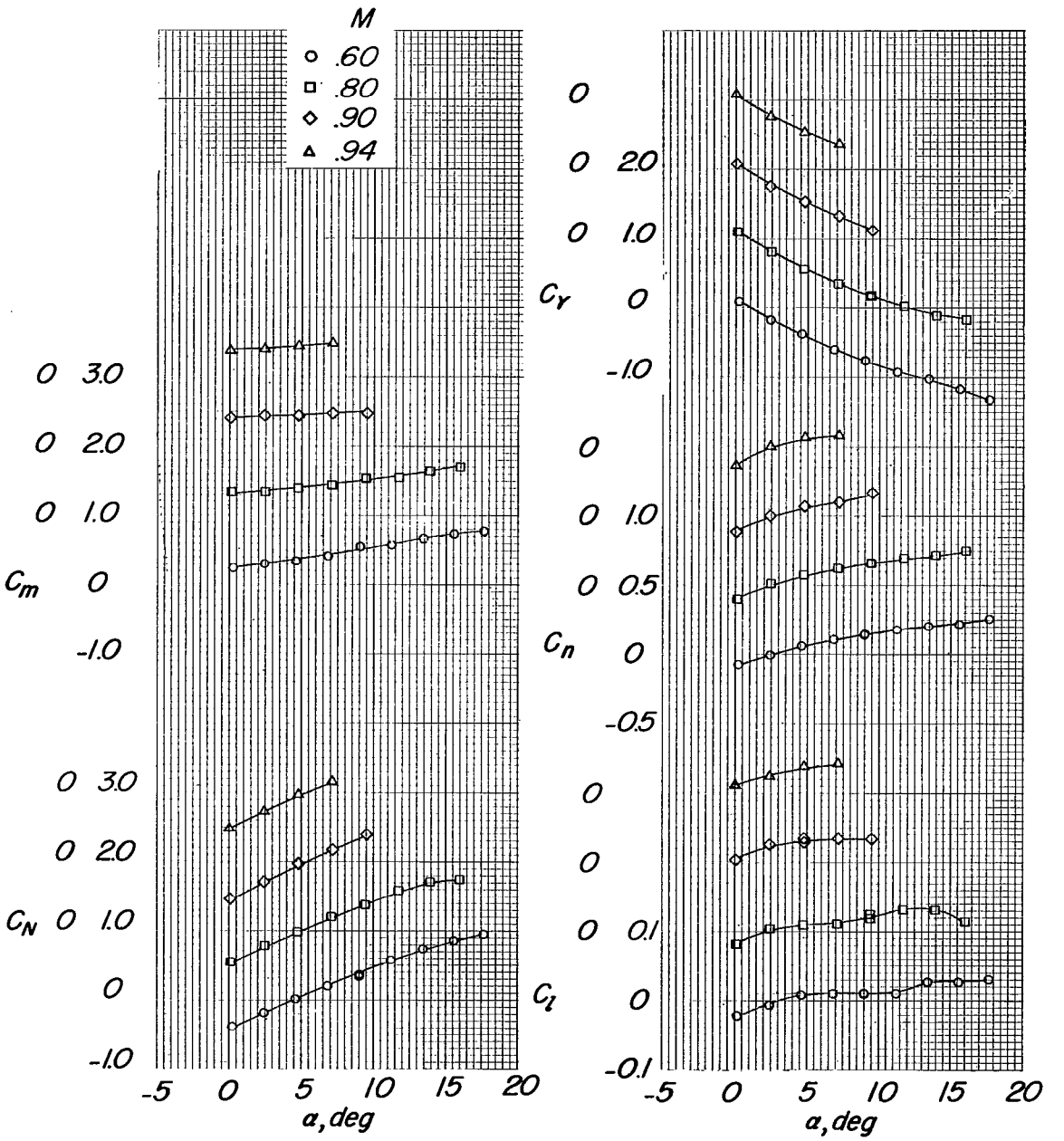

(d) x/c = 0.

Figure 8.- Continued.

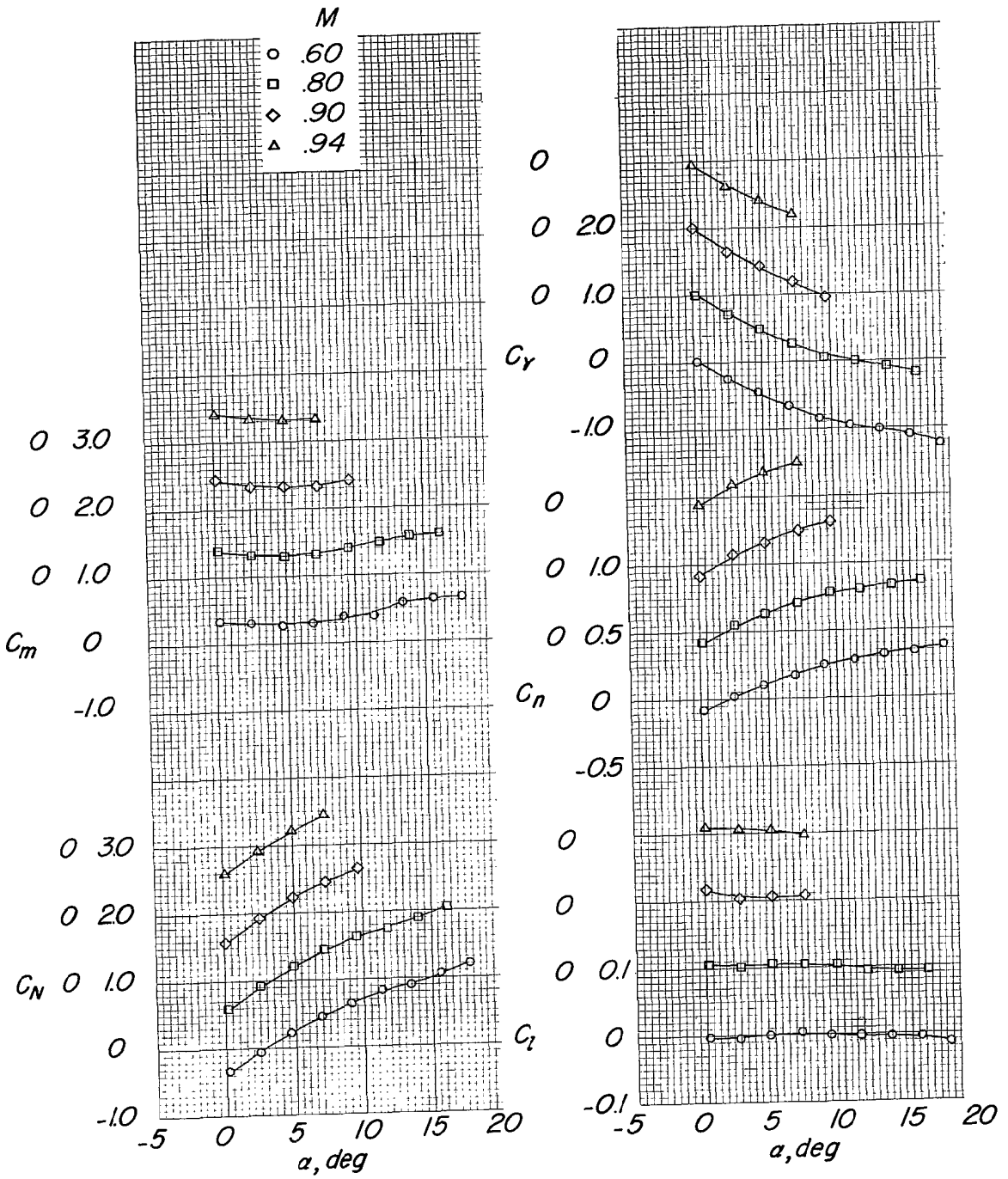

(e) x/c = -0.15.

Figure 8.- Continued.

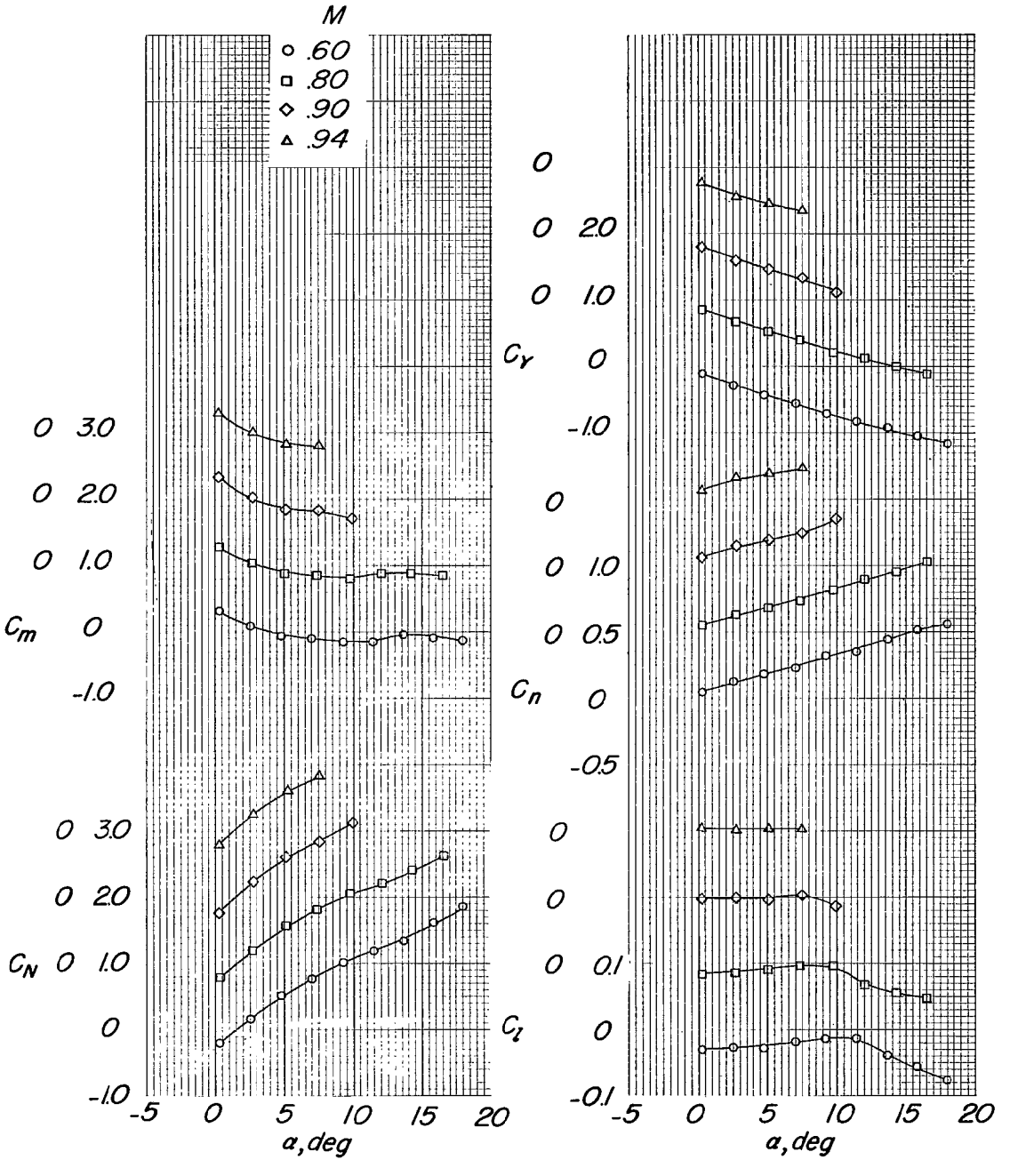

(f) x/c = -0.34.

Figure 8.- Continued.

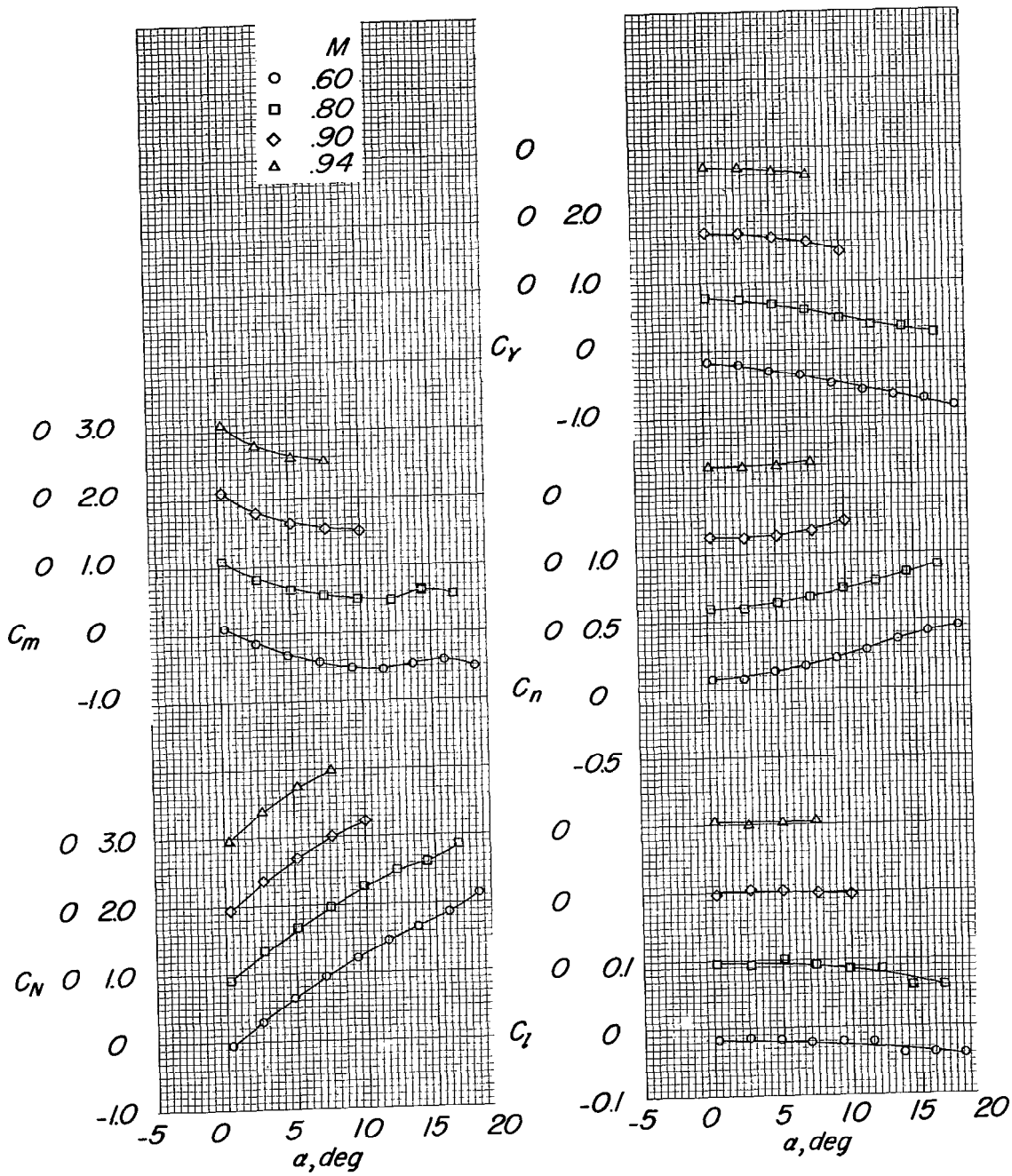

(g) x/c = -0.57.

Figure 8.- Continued.

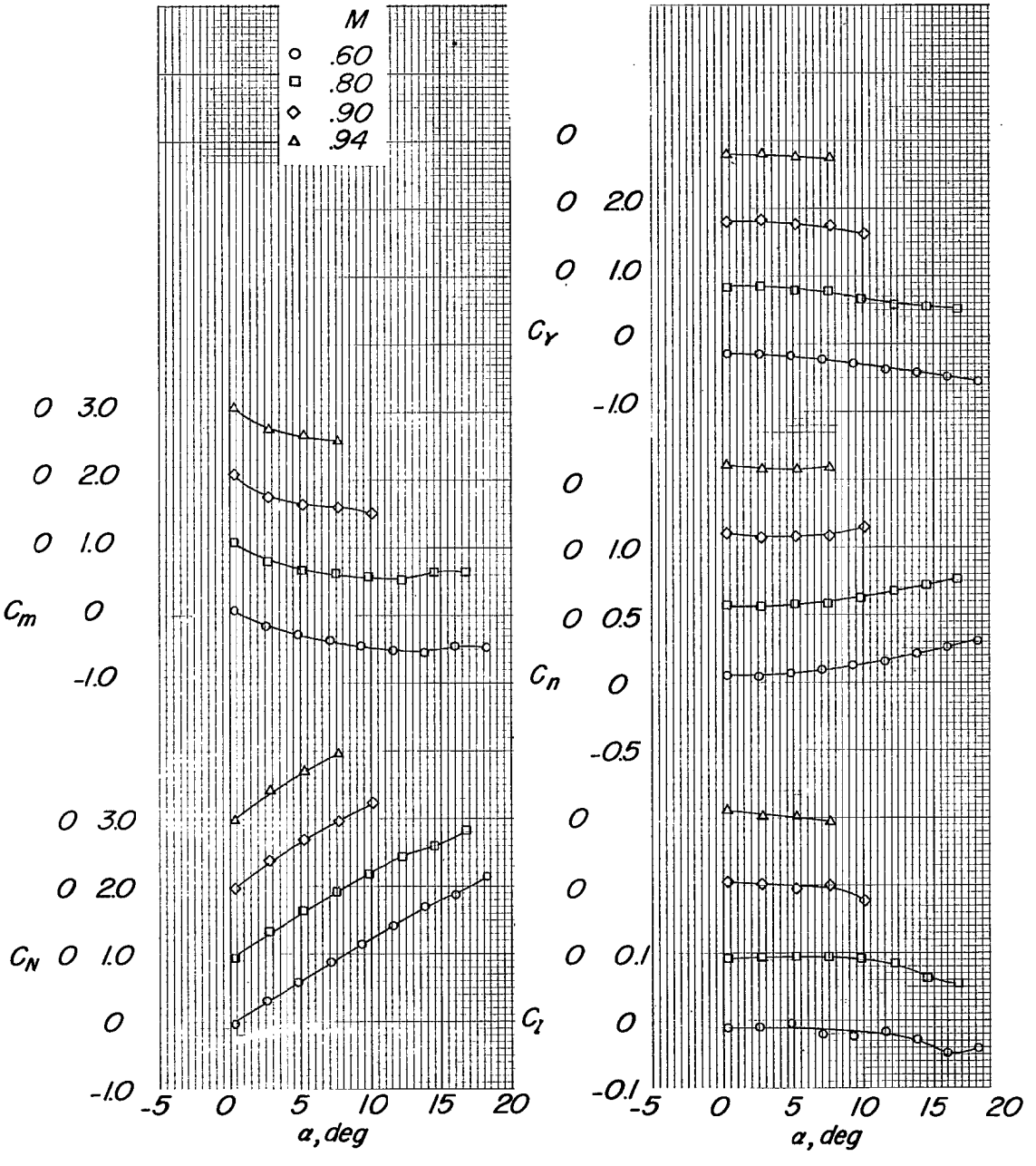

(h) x/c = -0.79.

Figure 8.- Continued.

[redacted]

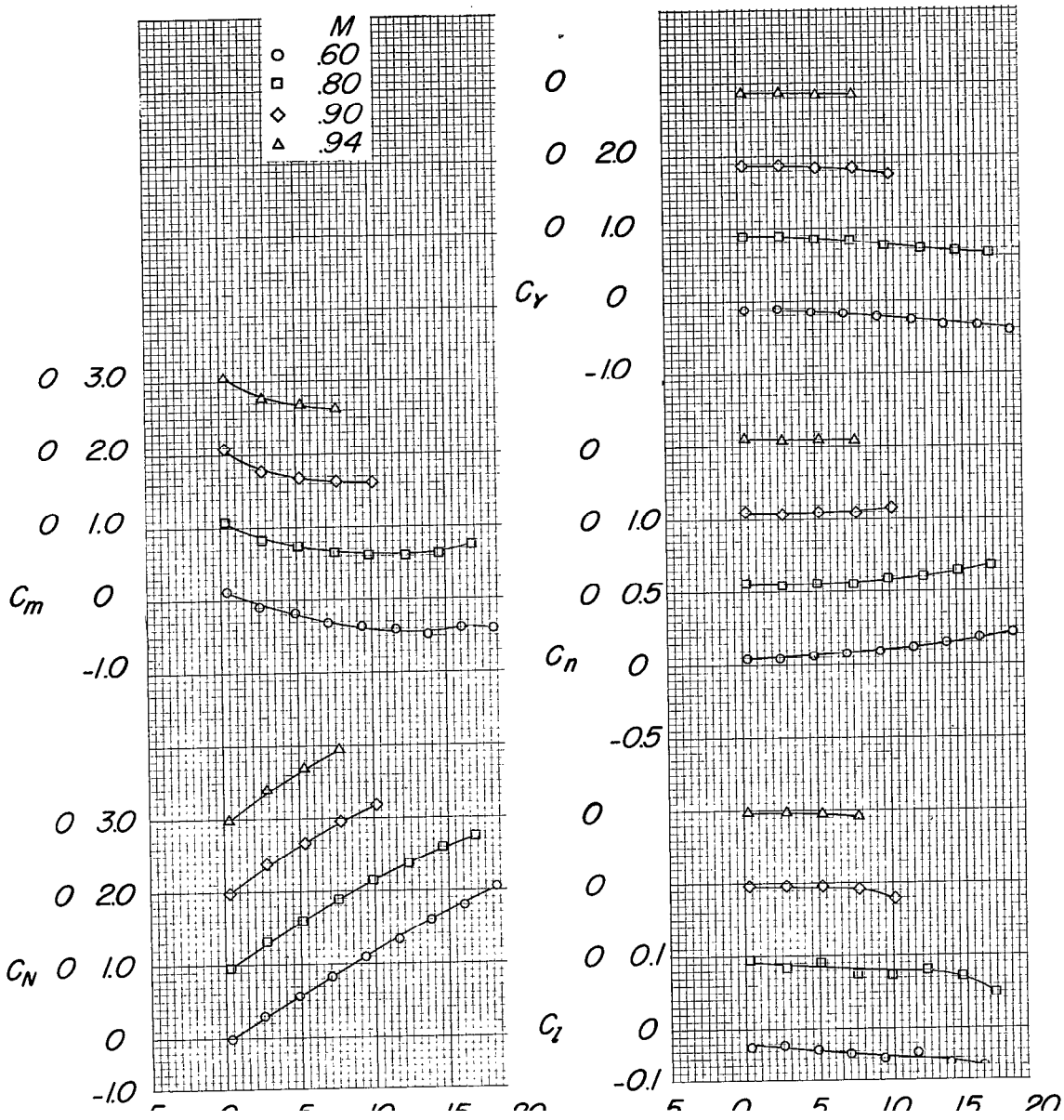
M
.60
.80
.90
.94
C_m
C_N
C_Y
C_n
C_l
0
3.0
2.0
1.0
-1.0
0.5
0.1
-0.5
-0.1
5
10
15
20

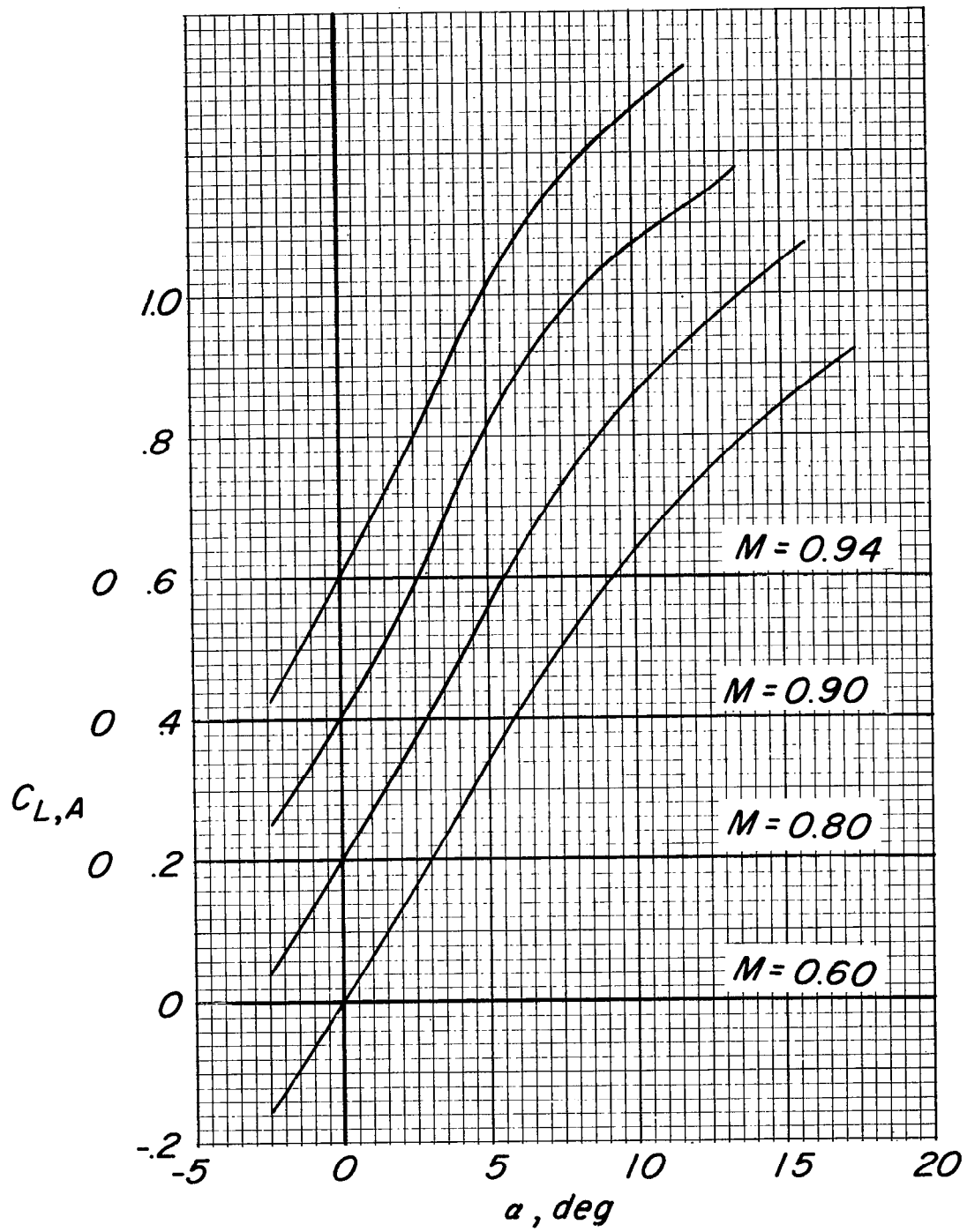

Figure 9.- Lift characteristics of isolated wing-fuselage combination.